ADVANCED SCIENCE Open Access
www.advancedscience.com

Rotaxane-Functionalized Dyes for Charge-Rectification in *p*-Type Photoelectrochemical Devices

*Tessel Bouwens, Tijmen M. A. Bakker, Kaijian Zhu, Annemarie Huijser, Simon Mathew, and Joost N. H. Reek**

A supramolecular photovoltaic strategy is applied to enhance power conversion efficiencies (PCE) of photoelectrochemical devices by suppressing electron–hole recombination after photoinduced electron transfer (PET). Here, the author exploit supramolecular localization of the redox mediator—in close proximity to the dye—through a rotaxane topology, reducing electron–hole recombination in *p*-type dye-sensitized solar cells (*p*-DSSCs). Dye $P_{Rotaxane}$ features 1,5-dioxynaphthalene recognition sites (DNP-arms) with a mechanically-interlocked macrocyclic redox mediator naphthalene diimide macrocycle (3-NDI-ring), stoppering synthetically via click chemistry. The control molecule $P_{Stopper}$ has stoppered DNP-arms, preventing rotaxane formation with the 3-NDI-ring. Transient absorption and time-resolved fluorescence spectroscopy studies show ultrafast (211 ± 7 fs and 2.92 ± 0.05 ps) PET from the dye-moiety of $P_{Rotaxane}$ to its mechanically interlocked 3-NDI-ring-acceptor, slowing down the electron–hole recombination on NiO surfaces compared to the analogue . *p*-DSSCs employing $P_{Rotaxane}$ (PCE = 0.07%) demonstrate a 30% PCE increase compared to $P_{Stopper}$ (PCE = 0.05%) devices, combining enhancements in both open-circuit voltages (V_{OC} = 0.43 vs 0.36 V) and short-circuit photocurrent density (J_{SC} = −0.39 vs −0.34 mA cm^{-2}). Electrochemical impedance spectroscopy shows that $P_{Rotaxane}$ devices exhibit hole lifetimes (τ_h) approaching 1 s, a 16-fold improvement compared to traditional I^-/I_3^--based systems (τ_h = 50 ms), demonstrating the benefits obtained upon nanoengineering of interfacial dye-regeneration at the photocathode.

1. Introduction

Dyes and pigments featuring rotaxane topologies are known in the scientific community and find application as nanoscale switches in molecular electronics amongst others.[1–5] In this work, we investigate a supramolecular photovoltaics approach to rectify charge propagation in solar cells through the use of rotaxane sensitizers.

Supramolecular electronics is a nascent sub-field of molecular electronics and has the potential to benefit from weak, non-covalent interactions between the components to (pre)organize their spatial positions to promote charge transport within molecular electronic devices.[6–15] While the development of supramolecular electronics is a thriving field,[16–22] the topic of supramolecular photovoltaics is scarcely explored. Recently, a self-assembled molecular *p*–*n* junction capable of a long charge-separated state lifetime (26 ms for the cathode), demonstrates that supramolecular candidates have the potential to replace silicon-based photovoltaics.[10,13,14,23,24]

The dye-sensitized solar cell (DSSC), first reported by Grätzel and O'Regan, is a thin-film technology for the direct conversion of solar energy to electricity.[25] In contrast to a silicon solar cell, light harvesting and charge separation events in a DSSC are decoupled and performed by different components. State-of-the-art devices exceed power conversion efficiencies (PCEs) of 15.2% for *n*-type DSSCs,[26] while the complementary *p*-type DSSC (*p*-DSSCs) remain subordinate with a current PCE record of 2.51%.[27,28] This disparity in performance precludes the widespread application of tandem DSSCs—especially to photoelectrochemical cells for solar fuel formation—and therefore, these efficiency losses must be addressed.[29–34]

Figure 1a illustrates the role of the different components in the forward electron propagation steps (Figure 1a, processes 1–4) (blue arrows) in *p*-DSSCs. Upon excitation of the dye (Figure 1a, process 1), hole injection takes place into the valence band (VB) of the semiconductor NiO (Figure 1a, process 2).[27] The subsequently reduced dye ($D^{\bullet-}$) transfers an electron to the redox mediator (Figure 1a, process 3), which diffuses towards the counter electrode (CE) (Figure 1a, process 4) for regeneration and

T. Bouwens, T. M. A. Bakker, S. Mathew, J. N. H. Reek
van 't Hoff Institute for Molecular Sciences
University of Amsterdam
Science Park 904, Amsterdam 1098 XH, The Netherlands
E-mail: j.n.h.reek@uva.nl
K. Zhu, A. Huijser
PhotoCatalytic Synthesis Group
MESA+ Institute for Nanotechnology
University of Twente
P.O. Box 217, Enschede 7500 AE, The Netherlands

The ORCID identification number(s) for the author(s) of this article can be found under https://doi.org/10.1002/advs.202306032

DOI: 10.1002/advs.202306032

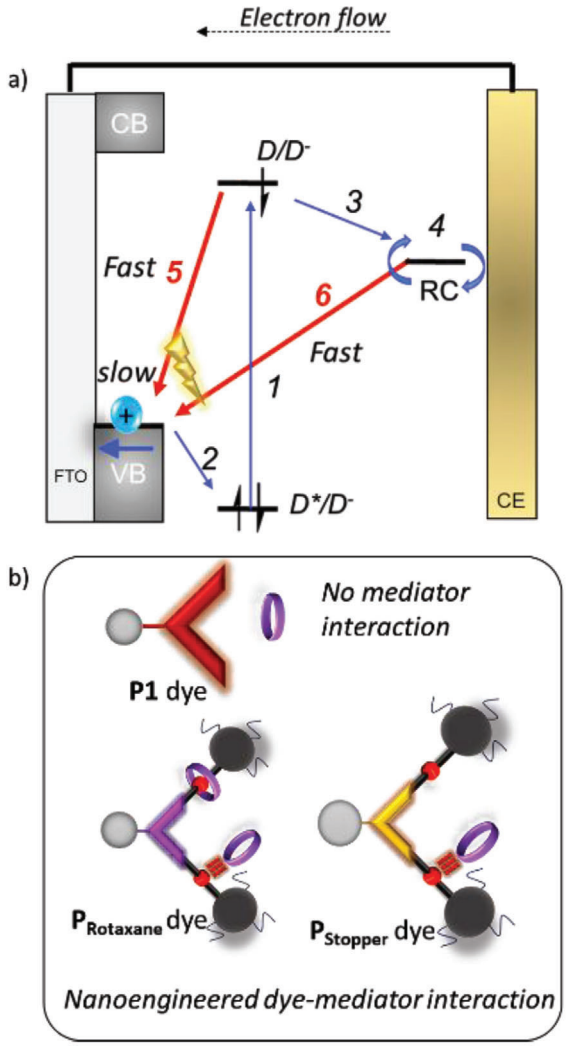

Figure 1. a) Schematic representation of forward electron propagation steps (1–4) (blue arrows) and recombination pathways (5, 6) (red arrows) leading to efficiency losses within *p*-DSSCs. FTO = fluorine-doped tin oxide; band; CB = conduction band; D = dye; RC = redox couple. a) Schematic representation of the benchmark system P1 dye (no mediator interaction) and $P_{Rotaxane}$/$P_{Stopper}$ dyes comprising nanoengineered dye-mediator interactions. $P_{Rotaxane}$ contains a permanently bound mediator as a built-in regeneration system and $P_{Stopper}$ is designed as a control to study the influence of a permanently bound mediator. The 3-NDI-ring is represented as a purple ring in the figure.

closing the cycle. However, after hole injection the charge carriers in $NiO^+|D^{\bullet-}$ can also recombine (Figure 1a, process 5). Additionally, the reduced mediator can react with NiO^+ sites (Figure 1a, process 6). These charge recombination pathways (Figure 1a, processes 5 and 6, red arrows) lead to efficiency losses within *p*-DSSCs.[27,35] The low PCE in *p*-DSSC can be attributed to severe electron–hole recombination caused by the extremely small hole diffusion coefficient in NiO (4×10^{-8} cm^2 s^{-1})[36] compared to 3–4 orders of magnitude faster (10^{-4} cm^2 s^{-1})[37] electron diffusion in TiO_2.[38–40] Therefore, fast and directional transport of charges after separation is crucial to promote forward electron propagation.

To compete with recombination pathways, dye–mediator interactions have been introduced in *p*-DSSCs to promote fast-forward electron transfer from the dye to the redox mediator by improving the proximity of this species, thereby enhancing the regeneration rate of the dye.[41–45] Previously, we introduced a pseudorotaxane strategy to pre-organize a tetracationic mediator close to the dye, elevating the photocurrent density (J_{SC}) tenfold.[46] Following this, we developed a new system where a neutral naphthalene diimide macrocycle (3-NDI-ring) forms pseudorotaxanes with the dye via the 1,5-dioxynaphthalene recognition sites (DNP-arms), and serves as redox mediator. After photoinduced electron transfer (PET), the 3-NDI-ring dethreads, effectively removing the charge away from the NiO^+–D^0 interface ($NiO^+|D$).[47] DSSCs based on such molecular mechanical systems show an increase in hole lifetime by a factor of two, enhancing the open circuit voltage (V_{OC}) and improving the PCE 5-fold compared to the benchmark system P1 which does not facilitate dye–mediator interactions.

In this work, we explore the potential of a new design approach that includes a rotaxane topology (**Figure 2**) and investigate the DSSC performance. The 3-NDI-ring is used as a redox mediator, possibly leading to mediator pre-organizations via weak interactions with the stoppered treats that have 1,5-dioxynaphthalene recognition sites not occupied with a permanent ring. We hypothesize that the $P_{Rotaxane}$ system featuring the nanoengineered strategy for dye-regeneration inspired by former dye–mediator interactions[46] will lead to the inhibition of recombination pathways 5 and 6 (Figure 1a) with concomitant promotion of forward electron propagation within the device.

2. Results and Discussion

2.1. Synthesis and Characterization of the Dyes

All compounds were prepared according to standard synthetic procedures described in Section S1.2, Supporting Information. Both the $P_{Rotaxane}$ and $P_{Stopper}$ dyes were fully characterized by NMR (^1H, ^{13}C, ^1H DOSY NMR), Electrospray Ionization High Resolution Mass spectrometry (ESI-HRMS), and spectrophotometric techniques. The large size of these dyes prompted the determination of the diffusion coefficient by ^1H DOSY NMR. Subsequent calculation of the molecular radius (*r*, Figure S11, Supporting Information) revealed $P_{Rotaxane}$ is larger ($r = 1.3$ nm) than $P_{Stopper}$ ($r = 1.1$ nm), ascribed to the presence of the 3-NDI-ring. The absorption and fluorescence spectra in MeCN solutions of $P_{Rotaxane}$, $P_{Stopper}$, and 3-NDI-ring are given in **Figure 3** and summarized in **Table 1**. The UV–vis spectrum of reference compound $P_{Stopper}$ features an absorption maximum at 462 nm attributed to intramolecular charge transfer (ICT) from the triphenylamine donor to the cyanoacrylate acceptor.[47] Additionally, $P_{Stopper}$ features absorption bands centered at 295, 311, and 326 nm, from the DNP-arms attached to the cyanoacrylate moiety.

Introduction of the electron acceptor 3-NDI-ring into the dye structure to yield $P_{Rotaxane}$ results in a slight red shift of the ICT absorbance to 465 nm compared to the control compound $P_{Stopper}$, likely originating from an additional charge-transfer band (@ 460 nm) upon interlocking of 3-NDI-ring and the DNP-arms. The emergence of the charge-transfer band upon combining 3-NDI-ring with the dihydroxynaphthalene recognition site was

Table 1. Optical and electrochemical properties of $P_{Rotaxane}$ and $P_{Stopper}$ (0.2 mM) in DCM (0.1 M $TBAPF_6$, glassy carbon working electrode, a leakless Ag/AgCl reference electrode, Pt wire counter electrode.

Dye	λ_{max} [nm]	$\epsilon \times 10^4$ [M^{-1} cm^{-1}]	$E_{0\text{-}0}$ [eV]	$E_{D/D}{}^+$	$E_{D/D}{}^-$	Dye coverage × 10^{-7} [mol cm^{-2}]
$P_{Stopper}$	462	6.6	2.29	1.10	−0.89	1.58
$P_{Rotaxane}$	467	4.2	2.30	1.17	−0.89	1.07

[a] Ferrocene/ferrocenium (Fc/Fc+) was added as an internal redox standard to determine the redox potentials versus NHE (E1/2 Fc/Fc+ = 630 mV vs NHE in MeCN[48] and 700 mV vs NHE in DCM).[49] [b] $E_{0\text{-}0}$ (eV) determined from the intersection between the normalized absorption and fluorescence spectra.

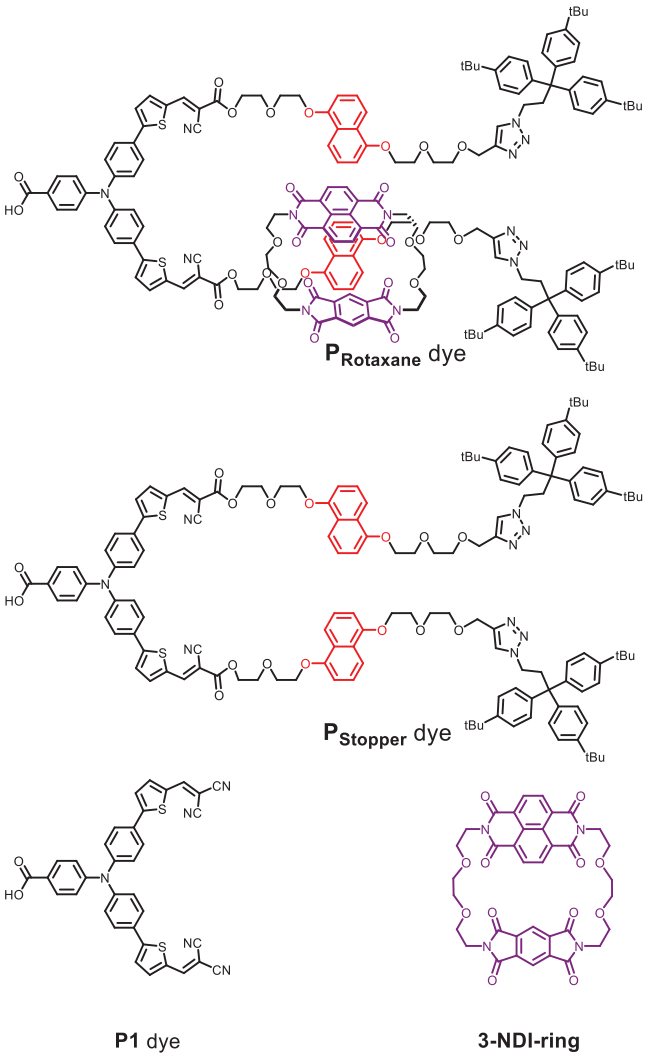

Figure 2. Molecular structures of the benchmark dye P1, the macrocyclic redox mediator 3-NDI-ring, $P_{rotaxane}$, and $P_{Stopper}$.

established in previous work,[47] where the mixing of 3-NDI-ring and $P_{STATION}$ prompts both broadening and red shifting of the UV–vis spectrum as a result of pseudorotaxane formation. In this work, we observe the same broadening/red shift phenomenon upon comparing the spectrum of $P_{Rotaxane}$ with $P_{Stopper}$. This similarity gives strong evidence for CT-band formation at 460 nm upon rotaxane formation. An additional absorption band in the $P_{Rotaxane}$ spectrum centered at 378 nm is ascribed to the mechanically interlocked 3-NDI-ring. These new absorption features in $P_{Rotaxane}$ coincide with a reduction (≈30%) in molar absorptivity (ϵ), ascribed to the mechanically interlocked 3-NDI-ring, and consistent with the earlier observation that host–guest complex formation can attenuate the molar absorptivity of the host.[50]

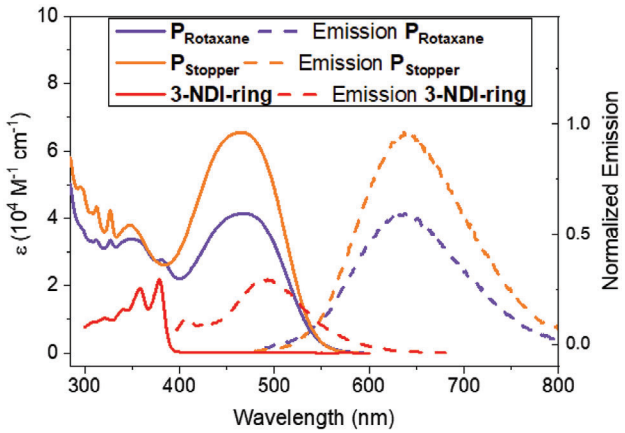

Figure 3. UV–vis spectra in MeCN of $P_{Rotaxane}$ (solid violet line), $P_{Stopper}$ (solid orange line), and compound 3-NDI-ring (red solid line) along with the normalized fluorescence spectrum upon excitation at λ_{max} ($P_{Rotaxane}$: violet dashed line, $P_{Stopper}$: orange dashed line, 3-NDI-ring: red dashed line). Fluorescence spectra are normalized with respect to the fluorescence intensity of $P_{Stopper}$ at 295 nm.

Insight into the redox properties of the $P_{Rotaxane}$, $P_{stopper}$, and 3-NDI-ring were obtained by cyclic voltammetry with the results summarized in Table 1. The reduction potential of $P_{Stopper}$ (−0.89 vs NHE, **Figure** 4a) is typical for P1-derived dyes (P1 = −0.77 V vs NHE in MeCN).[46] The small difference in potential is attributed to the respective acceptor strength (i.e., cyanoacrylate in $P_{Rotaxane}$, and $P_{Stopper}$ vs (dicyano)vinyl in P1). The electrochemistry of 3-NDI-ring includes four reduction events (Figure 4b), attributed to two, individual double-reduction events at the NDI (at −0.35 and −0.71 V vs NHE) and pyromellitic electron-accepting moieties within 3-NDI-ring (at −0.81 and −1.3 V vs NHE). The cyclic voltammogram of $P_{Rotaxane}$ displays multiple reduction events between -0.5–1.4 V, ascribed to both the presence of the dye and the 3-NDI-ring. The reduction events observed for $P_{Rotaxane}$ are clearly shifted in comparison to the free 3-NDI-ring. The reduction events of the 3-NDI-ring moiety within $P_{Rotaxane}$ include double-reduction events at the NDI (at −0.50 and −0.80 V vs NHE) and pyromellitic electron-accepting moieties within 3-NDI-ring (at −0.92 V, fourth reduction not visible with a CV but is clearly demonstrated by DPV to appear at −1.4 V vs NHE, Figure S23, Supporting Information).

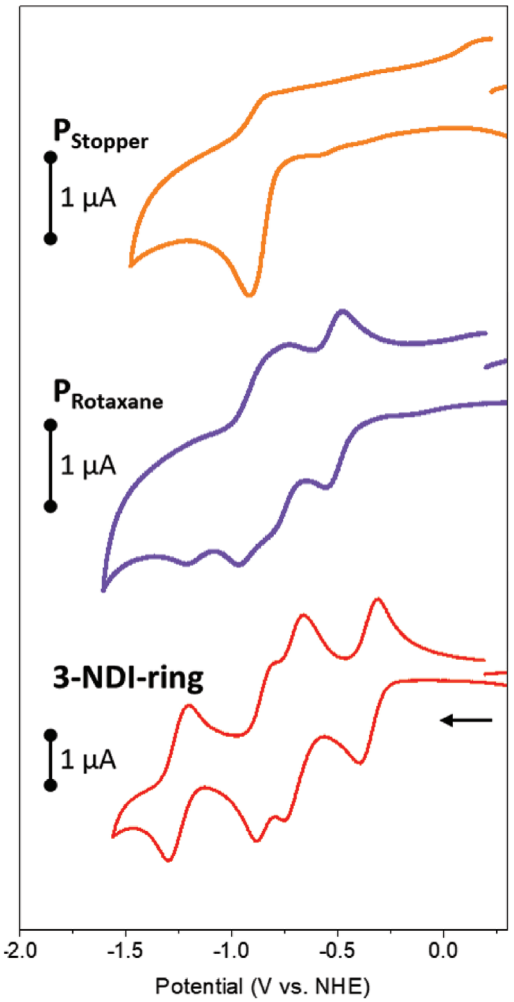

Figure 4. Cyclic voltammograms (0.1 M $TBAPF_6$ in DCM, 0.1 V s^{-1}) of $P_{Stopper}$ (orange line), $P_{Rotaxane}$ (violet solid line) (0.2 mM each), and 3-NDI-ring (red line) (0.5 mM). The arrow indicates the scanning direction. Note: The last reduction of 3-NDI-ring of $P_{Rotaxane}$ cannot be discerned through CV but is visible through differential pulse voltammetry (DPV, Figure S23, Supporting Information).

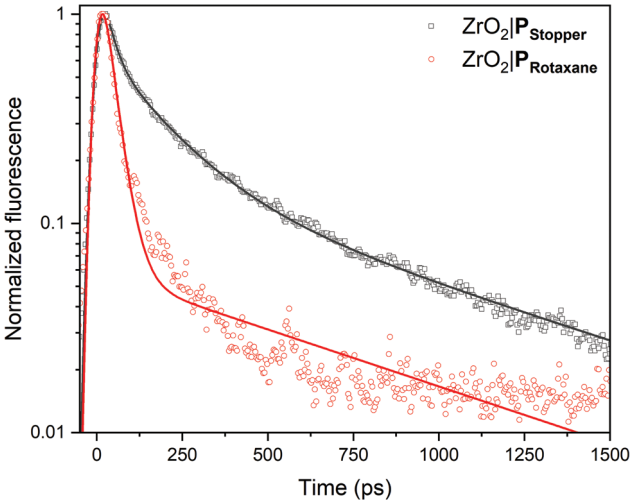

Figure 5. Decay of the normalized fluorescence signal at 615 nm ($\lambda_{exc.}$ = 532 nm) and fits for both $ZrO_2|P_{Stopper}$ and $ZrO_2|P_{Rotaxane}$. Note that the fluorescence of the latter is quenched, negatively affecting the signal-to-noise ratio and quality of the fit.

2.2. Ultrafast Spectroscopy Studies

Photoinduced charge propagation in $P_{Rotaxane}$ that occurs upon installing a permanently-bound redox mediator was further investigated by time-resolved fluorescence and femtosecond transient absorption (fs-TA) spectroscopy measurements using FTO glass substrates with layers of the $P_{Rotaxane}$ and $P_{Stopper}$ dyes on ZrO_2 and NiO immersed in a supporting electrolyte (1.5 mL, 1 M LiTFSI valeronitrile/MeCN, v/v, 15:85).

To study the occurrence of intramolecular electron transfer from $P_{Rotaxane}$ to the interlocked 3-NDI-ring on solid substrates, we conducted time-resolved fluorescence experiments ($\lambda_{exc.}$ = 532 nm) on $ZrO_2|P_{Rotaxane}$ and $ZrO_2|P_{Stopper}$. **Figure 5** demonstrates the decay of the normalized fluorescence signal at 615 nm for both $ZrO_2|P_{Stopper}$ and $ZrO_2|P_{Rotaxane}$. Compared to $ZrO_2|P_{stopper}$, the fluorescence of $ZrO_2|P_{rotaxane}$ is quenched, demonstrating that fast electron transfer from the dye part of $P_{Rotaxane}$ to the 3-NDI-ring indeed takes place. The associated time constant (listed in Figure S27 and Table S2, Supporting Information) for τ_1 is ~30 ps, while the small fluorescence signal that remains (Figure S27d, Supporting Information) is most likely due to the emission of $P_{Rotaxane}$ that has not undergone electron transfer (τ_2 ~800 ps). In the case of $ZrO_2|P_{Stopper}$, the slower fluorescence decay indicates that the fluorescence is not quenched and no fast photoinduced electron transfer takes place (τ_1 = 25.2 ± 0.1 ps; τ_2 = 166.6 ± 0.2 ps; τ_3 = 823.6 ± 0.8 ps).

To further understand the electron propagation upon photoexcitation of $P_{Rotaxane}$ and $P_{Stopper}$ dyes on the metal oxide substrates, we also conducted fs-TA experiments. Previously, we established that the transient behavior of P1 as a benchmark system under analogous conditions is consistent with reports from the literature.[47,51–53] In the case of NiO|P1, four distinct time constants are apparent from photophysical modeling, indicating that biphasic photoinduced hole injection (ultrafast, i.e., within a few hundred fs, and in 1–2 ps) is followed by a fast (≈5–10 ps) and a slow (>100 ps) charge recombination step.[51–53] The fs-TA data of $P_{Rotaxane}$ and $P_{Stopper}$ in solution (Figure S25, Supporting Information) and on ZrO_2 (Figure S26, Supporting Information) are discussed in Section S2.2 of the Supporting Information.

The fs-TA spectra of $NiO|P_{Rotaxane}$ at various time delays after 480 nm excitation are presented in **Figure 6a**, and further detailed in Section S2 of the Supporting Information. Analogous to the NiO|P1 benchmark system,[51–53] the negative signal < 560 nm is due to ground state bleach, while the photoinduced absorbance around 575 nm (black dashed line) can be assigned to $P_{Rotaxane}^*$ and $P_{Rotaxane}^{\bullet-}$. The latter likely has a slightly red-shifted absorption band relative to $P_{Rotaxane}^*$ and is formed due to photoinduced hole injection into NiO, either within a few hundred fs or in 1–2 ps.[51–53] This assignment is in line with the spectroelectrochemical measurements of $P_{Rotaxane}$ that show a 22 nm red- shift of $P_{Rotaxane}^{\bullet-}$ compared to $P_{Rotaxane}$ (Figure S24, Supporting Information).

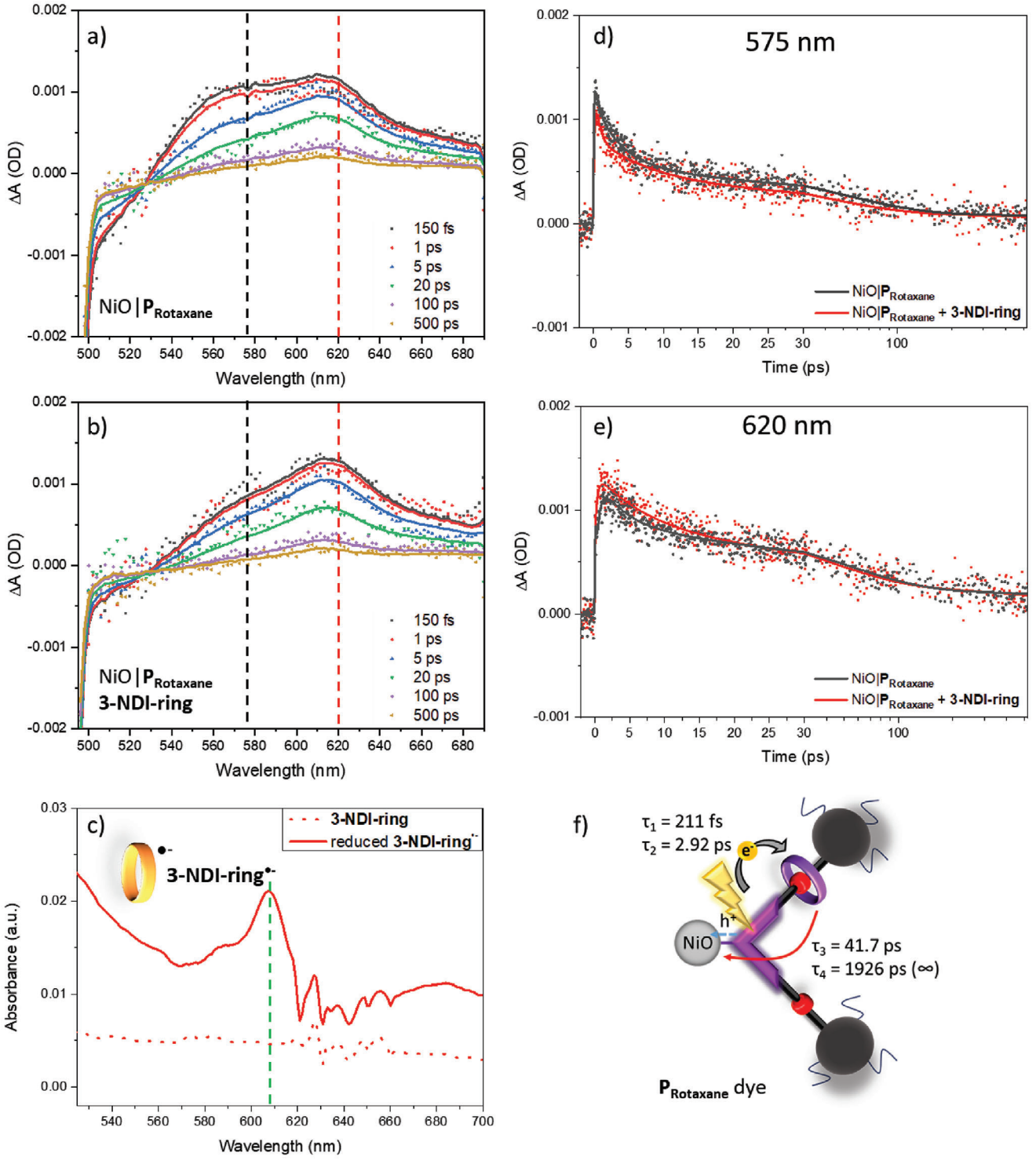

Figure 6. Transient absorption (TA, $\lambda_{exc.} = 480$ nm) data and fits (see Section S2, Supporting Information for details) of $P_{Rotaxane}$ on NiO in supporting electrolyte (1.5 mL, 1 M LiTFSI valeronitrile/MeCN, 15:85) in absence and presence of the 3-NDI-ring (5.9 mM). a) TA spectra at given time delays in the absence of the 3-NDI-ring. The photoinduced absorbance of NiO|$P_{Rotaxane}$ around 575 nm is indicated with a black dashed line and indicative of a combination of $P_{Rotaxane}^{*}$ and $P_{Rotaxane}^{\bullet -}$; b) TA spectra at given time delays in the presence of the 3-NDI-ring; c) Spectroelectrochemistry of the 3-NDI-ring (dotted green line), which shows an absorption band around 608 nm when the 3-NDI-ring$^{\bullet -}$ is formed (solid red line); d) Kinetic traces at 575 nm with (red) and without 3-NDI-ring present in the electrolyte (black); e) Kinetic traces at 620 nm with (red) and without 3-NDI-ring present in the electrolyte (black); f) Schematic representation of charge transfer processes following excitation of the $P_{Rotaxane}$ dye in absence of free 3-NDI-ring.

The fs-TA spectra of NiO|$P_{Rotaxane}$ in the presence of the 3-NDI-ring shown in Figure 6b diverge significantly from the data presented in Figure 6a, with a more intense photoinduced absorbance around 620 nm. Based on the fluorescence quenching demonstrating photoinduced reduction of the ring (Figure 5) and the spectroelectrochemistry data (3-NDI-ring$^{\bullet-}$ λ_{max} ≈608 nm, Figure 6c, green dashed line), we assign this additional TA signal to the 3-NDI-ring$^{\bullet-}$. The observed ~12 nm red- shift of the interlocked 3-NDI-ring$^{\bullet-}$ moiety in NiO|$P_{Rotaxane}^{\bullet-}$ (with respect to free diffusing 3-NDI-ring$^{\bullet-}$) is likely due to photoinduced charge separation with the NiO, and could also be a consequence of the interlocked 3-NDI-ring$^{\bullet-}$ (vs free 3-NDI-ring$^{\bullet-}$).[54–56]

The TA signal at 620 nm fully develops within 150 fs after photoexcitation, indicating that ultrafast hole injection from the $P_{Rotaxane}$ dye into the valence band of NiO coincides with the formation of the 3-NDI-ring$^{\bullet-}$. Intramolecular charge transfer towards the ring is hence likely also an ultrafast process, photophysical modeling gives a time constant of 210 ± 7 fs. The intensity of the photoinduced absorbance at ≈575 nm decreases over time relative to the photoinduced absorption at ≈620 nm, which can be ascribed to slow (2.92 ± 0.05 ps) hole injection from $P_{Rotaxane}$ into the NiO coupled to electron transfer to the 3-NDI-ring. The ground state bleach beyond these times indicates that not all excited complexes give both hole injection and electron transfer with these time constants, which may be a result of structural inhomogeneity of the $P_{Rotaxane}$ dye, as further explained in Section S2.2, Supporting Information. Subsequent decay of the 575 and 620 nm photoinduced absorption bands, further illustrated by the kinetic traces in Figure 5d,e, indicates charge recombination. Details regarding the photophysical modeling, resulting in the fits included in Figure 6, are given in Section S2, Supporting Information. In this model, photoinduced hole injection partly occurs simultaneously with 3-NDI-ring reduction, while the other dye radical anions give slower ring reduction (time constants in Section S2.2, Supporting Information), possibly due to structural inhomogeneity. The obtained charge transfer times are illustrated in Figure 6f.

In the 3-NDI-ring containing electrolyte (Figure 6b), the fs-TA spectra are nearly identical to those in the electrolyte without added 3-NDI-ring (Figure 6a), featuring two photoinduced absorbance bands centered around 575 and 620 nm. The comparison of kinetic traces indicates that in the 3-NDI-ring containing electrolyte the transient signals at 575 nm (Figure 6d) and 620 nm (Figure 6e) decay a little bit faster. Photophysical modeling seems to suggest slightly faster ring reduction and charge recombination (Table S4, Supporting Information, τ_2, τ_3, τ_4). Though the differences are small, they may originate from the 3-NDI-ring in the electrolyte acting as an electron acceptor, that is, the respective intra- and inter-molecular electron transfer processes cannot be decoupled and direct transfer to the unbound redox mediator cannot be excluded.

2.3. Proposed Electron Propagation within NiO|$P_{Rotaxane}$

With the photophysical properties and electrochemical data in hand, we can construct an energy diagram and predict how the electrons propagate within the $P_{Rotaxane}$ system (**Figure 7**). The electrochemical studies reveal that the thermodynamics of

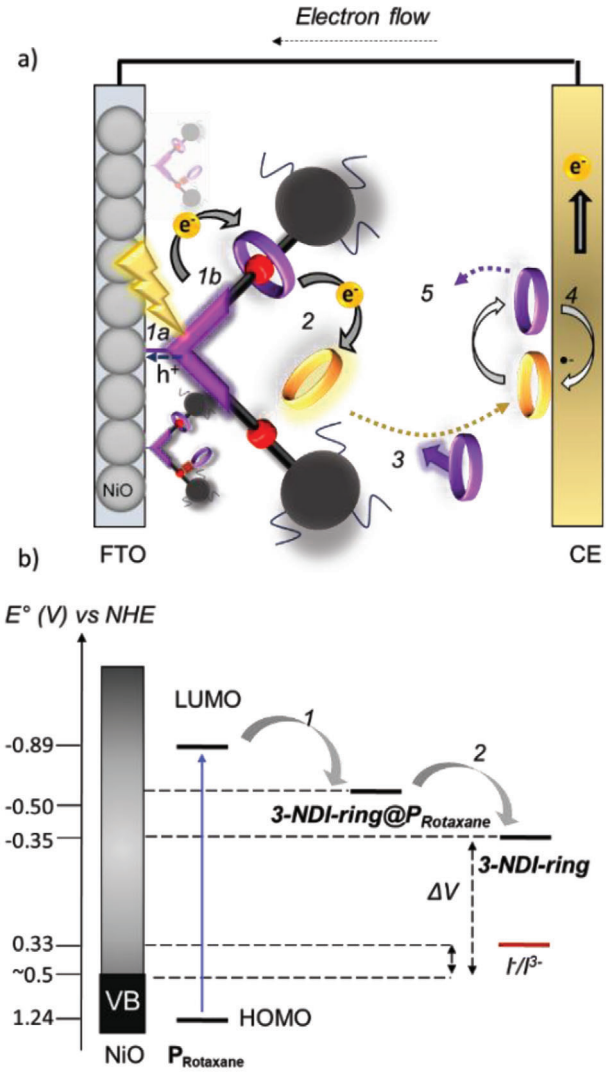

Figure 7. a) Schematic representation of charge propagation of the rotaxane-based *p*-DSSC. b) Schematic energy diagram for the *p*-DSSC based on the $P_{Rotaxane}/P_{Stopper}$ dyes. Upon excitation of the $P_{Rotaxane}$ hole injection takes place (process 1a) and simultaneously the mechanically bound 3-NDI-ring@$P_{Rotaxane}$ is reduced (process 1b). Then, the reduced 3-NDI-ring$^{\bullet-}$@$P_{Rotaxane}$ is able to reduce the 3-NDI-ring present in the bulk solution (process 2). Energy levels are represented in V versus NHE.

the rotaxane-dye support electron transfer from the reduced dye $P_{Rotaxane}^{\bullet-}$ to the interlocked 3-NDI-ring. As the redox potential of the "free" 3-NDI-ring is less negative than of the interlocked 3-NDI-ring, electron transfer is exergonic from the anionic interlocked 3-NDI-ring$^{\bullet-}$ and freely diffusing 3-NDI-ring in the bulk electrolyte. Furthermore, fs-TA results demonstrate the fast kinetics of electron transfer from the reduced dye $P_{Rotaxane}^{\bullet-}$ to the interlocked 3-NDI-ring and the effect of a second "free" 3-NDI-ring possibly acting as an electron acceptor.

Figure 7a illustrates the proposed rotaxane-based *p*-DSSC consisting of the $P_{Rotaxane}$ dye. The molecular structure of $P_{Rotaxane}$ (Figure 2) contains one DNP-arm that is mechanically bound to the 3-NDI-ring as the tris(4-*t*-butylphenyl)methyl stoppers prevent slippage of the macrocyclic 3-NDI-ring. The qualitative

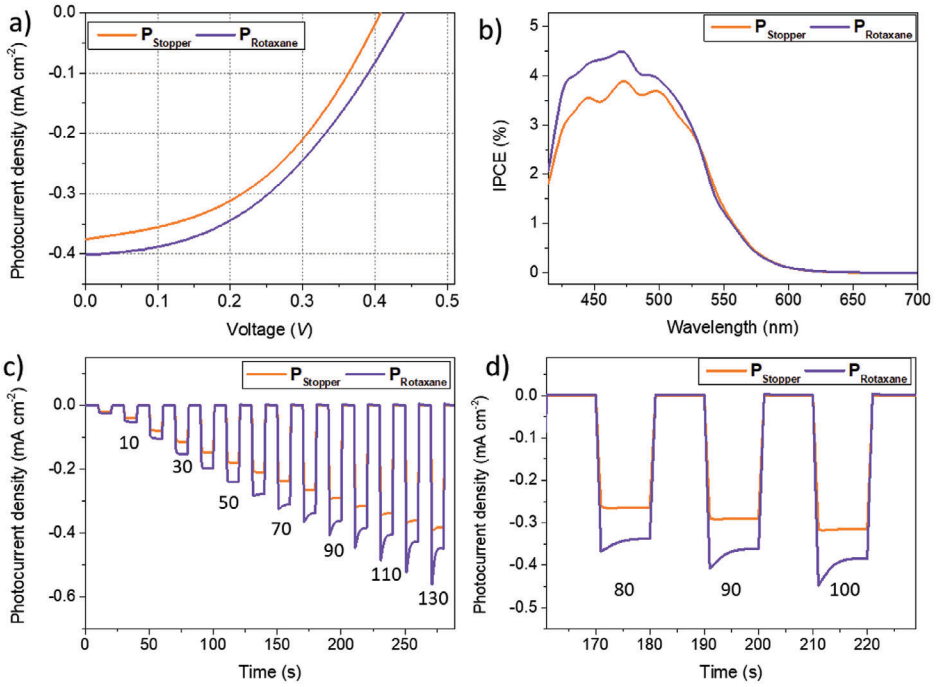

Figure 8. Photovoltaic performances of the devices based on the $P_{stopper}$ (orange line) and the $P_{Rotaxane}$ dye (violet line) with the 3-NDI-ring as redox mediator (25 mM 3-NDI-ring/3-NDI-ring$^{\bullet-}$ 1:1 in 1 M LiTFSI valeronitrile/MeCN, 15:85). a) *J–V* curves of the on the $P_{stopper}$ (orange line) and the $P_{Rotaxane}$ dye (violet line). b) Photocurrent action spectrum. c) Chopped light amperometry at different light flux varying from 0.05–1.3 W cm^{-2} with on/off cycles of 10 s. d) Zoom of chopped light amperometry at 80, 90, and 100 mW cm^{-2} clearly showing tailing behavior indicative of mass transfer limitation.

binding studies described in Section S1.5, Supporting Information estimated from UV–vis and ^{1}H NMR binding data, suggest that the other DNP-arm could be available for an interaction with a second 3-NDI-ring by an alternate binding mode (vide supra). The interaction of the second 3-NDI-ring might be based on π-stacking between the DNP-arm and the naphthalene diimide. According to our fs-TA studies, upon photoexcitation of the dye, the electron is transferred very quickly to the proximal 3-NDI-ring within the $P_{Rotaxane}$ structure (Figure 7a, step 1). This process likely occurs simultaneously with the hole transfer to the NiO (process 1a). The interlocked 3-NDI-ring$^{\bullet-}$ anion is able to reduce a 3-NDI-ring from solution, that may be preorganized via weak interactions with the adjacent DNP-arm (Figure 7a, step 2). This free 3-NDI-ring$^{\bullet-}$ (Figure 7a, step 3) is subsequently regenerated at the counter electrode (Figure 7a, step 4). The $P_{Stopper}$ reference dye features both DNP-arms for binding with 3-NDI-ring via π–interactions but no rotaxane-bound 3-NDI-ring allowing it to function as a reference to investigate the role of the mechanically-bound mediator in $P_{Rotaxane}$. Having established that both the thermodynamics and kinetics are in favor of forward electron propagation, the influence of the rotaxane design can be investigated in the *p*-DSSC.

2.4. Photovoltaic Performance

Next, we explored the effect of the rotaxane topology on the performance of the *p*-DSSC. The *p*-DSSCs were prepared using screen-printed NiO photocathodes (3.5 µm, 0.2 cm^{-2}) that were sensitized with $P_{Stopper}$ or $P_{Rotaxane}$ in MeCN solution (0.15 mM) for 16 h. Dye uptake experiments (Section S1.6, Supporting Information.) revealed that the surface coverage of $P_{Stopper}$ ($\Gamma = 1.58 \times 10^{-7}$ mol cm^{-2}) is ≈50% higher than that of $P_{Rotaxane}$ ($\Gamma = P_{Rotaxane}$ 1.07×10^{-7} mol cm^{-2}), which is expected based on the increase molecular size incurred by $P_{Rotaxane}$ upon rotaxane formation with 3-NDI-ring (r = 1.1 nm for $P_{Stopper}$ vs r = 1.3 nm for $P_{Rotaxane}$, Figure S11, Supporting Information).

Initial assessment of *p*-DSSC devices was performed using the I^-/I_3^- redox electrolyte (1 M LiI and 0.1 M I_2 in MeCN). We also fabricated *p*-DSSCs with the dye P1 as a benchmark system *p*-DSSC affording a PCE (0.061% ± 0.002%), comparable to the best performing analogous devices literature (0.075%) (see Section 3.6, Supporting Information).[57] The small discrepancies between our P1 cells and literature values are ascribed to the quality of the NiO, which is well known to vary based on several factors, such as nanoparticle size and Ni^{3+} impurities.[57,58]

The *p*-DSSCs were prepared employing the 3-NDI-ring electrolyte (25 mM 3-NDI-ring/3-NDI-ring$^{\bullet-}$, 1:1 in 1 M LiTFSI valeronitrile/MeCN, 15:85) with a 60 µm thermoplast frame. Poly(3,4-ethylenedioxythiophene) (PEDOT) counter electrode was employed instead of the typically used Pt, to take advantage of its lower charge transfer resistance against organic radical redox couples.[59] The photocurrent–voltage (*J–V*) characteristics (**Figure 8a**) of the *p*-DSSCs based on $P_{Rotaxane}$ and $P_{Stopper}$ with the 3-NDI-ring electrolyte were measured under AM 1.5G illumination (100 mW cm^{-2}), with the data summarized in **Table 2**. The *p*-DSSCs sensitized with $P_{Rotaxane}$ demonstrate an increase in performance compared to the analogue based on the $P_{Stopper}$

Table 2. Summary of the photovoltaic performance data for *p*-DSSC based on $P_{Stopper}$ and $P_{Rotaxane}$ under AM 1.5G illumination (0.1 W cm^{-2}) employing the 3-NDI-ring electrolyte (25 mM) in 1 M LiTFSI valeronitrile/MeCN, (15:85). The average performance ($N = 9$) is provided with the best-performing cell in brackets.

Dye	V_{OC} [V]	J_{SC} [mA cm^{-2}]	FF	PCE [%]
$P_{Stopper}$	0.36 ± 0.05 (0.41)	−0.34 ± 0.08 (−0.42)	0.41 ± 0.04 (0.45)	0.05 ± 0.02 (0.07)
$P_{Rotaxane}$	0.43 ± 0.04 (0.47)	−0.39 ± 0.03 (−0.40)	0.40 ± 0.03 (0.43)	0.07 ± 0.01 (0.08)

system demonstrating that the permanently present redox mediator as a dye design feature has an overall positive effect on the *p*-DSSC performance. Not only does $P_{Rotaxane}$ demonstrate a higher V_{OC} than $P_{Stopper}$ (0.43 vs 0.36 V, respectively), accompanying improvements to J_{SC} (0.39vs 0.34 mA cm^{-2}, respectively) result in a better PCE (0.07% vs 0.05% respectively). Furthermore, the incident photon-to-current efficiency (IPCE) of $P_{Rotaxane}$-based *p*-DSSC ($IPCE_{max}$ = 4.49% at 471 nm) is greater across the whole spectrum compared to $P_{Stopper}$ analogue ($IPCE_{max}$ = 3.88% at 474, Figure 8b). The difference between the *p*-DSSCs was further characterized by their photocurrent response upon varying light intensity, through chopped-light amperometry (Figure 8c,d). The *p*-DSSCs based on the $P_{Rotaxane}$ demonstrate a higher J_{SC} upon illumination at every light intensity from 414–700 compared to $P_{Stopper}$, which is which is in line with the *J*–*V* characterization (Figure 8a). The shape of the photocurrent response exhibits tailing where the signal decays, especially at higher J_{SC}, indicative of mass transfer limitations in the device from slow diffusion of the redox mediator hampering current generation.[60,61]

As the association of the 3-NDI-ring-mediator to $P_{Rotaxane}$ is weak (i.e., < 10 M^{-1}), diffusional processes dominate the behavior of the electrolyte, leading to a decrease in the amount of dye–mediator pre-organization. This tailing behavior was also observed in a former study where P1 was combined with 3-NDI-ring, having no supramolecular interaction. In case a supramolecular interaction is established between the dye and 3-NDI-ring by means of pseudorotaxane formation, the tailing behavior disappears by pre-organization of the mediator to the dye.[47]

2.5. Electrochemical Impedance Spectroscopy

To further understand the suppression of recombination in devices based on $P_{Rotaxane}$ electrochemical impedance spectroscopic (EIS) measurements were carried out at different light intensities. The results were analyzed using the transmission line model with the addition of a Warburg element to simulate electrolyte diffusion (See Section S3.7, Supporting Information).[62] The chemical capacitance C_μ reveals a slight upwards (28 mV) shift of the valance band for $P_{Rotaxane}$ (Figure S35, Supporting Information), which can be assigned to the difference in dye loading, leaving less NiO sites exposed to interact with ions present in the electrolyte.[62,63] The recombination resistance (R_{REC}) is double for $P_{Rotaxane}$ devices (40.8×10^3 Ω cm^{-2} at 100 mV) compared to those based on $P_{Stopper}$ (21.8×10^3 Ω cm^{-2} at 100 mV) implying less recombination occurs at the NiO–dye interface in the $P_{Rotaxane}$ *p*-DSSCs. This difference in R_{REC} (at any given voltage) translates into a 50% increase in hole lifetime for $P_{Rotaxane}$ *p*-DSSCs (811 ms at 100 mV) compared to devices based on $P_{Stopper}$ (527 ms at 100 mV). The decrease in recombination in the $P_{Rotaxane}$ system compared to $P_{Stopper}$, translates into an extended hole lifetime, leading to a higher V_{OC}, J_{SC}, and PCE.

To demonstrate the effect of the rotaxane-based dye design on the charge recombination, the hole lifetimes (at 100 mV) of the devices based on the different P1-derived dyes $P_{Rotaxane}$ and $P_{Stopper}$ are summarized together with PCE and dye loading in **Table 3**. The *p*-DSSC devices using I^-/I_3^- electrolytes were also assessed to serve as a point of reference, being a system exhibiting no diffusional limitation.

The benchmark *p*-DSSC employing P1 and I^-/I_3^- electrolyte affords a τ_h of 113 ms, which is close to that reported in literature (356 ms in literature[63]), the difference ascribed to the quality of the NiO, which is known to vary based on several factors, such as nanoparticle size[57]). In comparison, the $P_{Rotaxane}$ and $P_{Stopper}$ dyes combined with I^-/I_3^- electrolytes demonstrate shorter hole lifetimes (50 and 29 ms respectively). These low τ_h values indicate severe recombination at the Dye–NiO interface, in line with the lower dye loading in these cells, leaving many NiO^+-sites exposed ($\Gamma = 1.58 \times 10^{-7}$ and 1.07×10^{-7} mol cm^{-2} for $P_{Rotaxane}$ and $P_{Stopper}$ respectively, compared to $\Gamma = 3.24 \times 10^{-7}$ mol cm^{-2} for P1). While these hole lifetimes are much lower compared to the electron lifetimes observed for typical *n*-DSSCs (≈3500 ms[63]), the discrepancy in charge carrier lifetime is expected given the severe charge recombination in these *p*-type DSSCs using I^-/I_3^- as an electrolyte.

Due to the limited solubility of the 3-NDI-ring, the *p*-DSSCs based on this mediator were prepared with a 40 times lower redox mediator concentration compared to those based on I^-/I_3^- as electrolyte. The *p*-DSSCs employing the 3-NDI-ring (25 mM) as electrolyte demonstrate much longer hole lifetimes compared to cells with the 1 M I^-/I_3^- as electrolyte. We observe that a short hole lifetime results in a lower PCE, consistent with the data of P1 devices using 25 mM I^-/I_3^- electrolyte.

A trend in the hole lifetime **P1 < $P_{Stopper}$ < $P_{Rotaxane}$** was observed in all devices, attributed to the supramolecular localization of the redox mediator in close proximity to the dye through a rotaxane-topology, increasing the sensitizer regeneration rate during device operation. The hole lifetimes increase by a factor of 16–18 compared to the I^-/I_3^- cells, despite the lower electrolyte (25 mM for 3-NDI-ring vs 1 M for I^-/I_3^-) concentration. A direct comparison between the 1 M I^-/I_3^- electrolyte and 3-NDI-ring

Table 3. Overview of hole lifetimes (τ_h) of different systems at 100 mV. The higher hole lifetime of the systems in this study originates from the suppression of charge recombination at the NiO|Dye interface.

Dye	Dye loading [Γ, $\times 10^{-7}$ mol cm^{-2}]	Electrolyte	PCE [%]	τ_h [ms, at 100 mV]
$P_{Stopper}$ [a]	1.07	25 mM 3-NDI-ring	0.05	527
		1 M I^-/I_3^-	0.03	28.5
$P_{Rotaxane}$ [a]	1.58	25 mM 3-NDI-ring	0.07	811
		1 M I^-/I_3^-	0.04	49.7
P1 [b]	3.24	25 mM 3-NDI-ring	0.01	324
		1 M I^-/I_3^-	0.06	113
		25 mM I^-/I_3^-	0.01	N/A

[a] This work [b] Former work.[47]

(25 mM) is inadequate, because of the difference in electrolyte concentration and molecular size. However, we do observe a general trend when moving from 1 M I^-/I_3^- electrolyte to 3-NDI-ring (25 mM) in higher τ_h, leading to improved V_{OC} and enhanced PCE (Table 3).

The diffusion (D_e) of redox mediators in devices employing macrocycles (25 mM 3-NDI-ring, $D_e = 1.4 \times 10^{-10}$ m^2 s^{-1}) is approximately four times slower than for I^-/I_3^- (1 M, $D_e = 4.85 \times 10^{-10}$ m^2 s^{-1}) (see Section S3.11, Supporting Information). This difference in diffusion is in line with the mass-transfer limitations observed in the chopped light experiments (Figure 8c). Furthermore, as the r of iodide ($r = 0.2$ nm)[64] is 3.5 times smaller than 3-NDI-ring ($r = 0.7$ nm, Figure S11, Supporting Information) the former is expected to experience faster diffusion kinetics.

Despite the slow diffusion kinetics, the 3-NDI-ring-based *p*-DSSCs using the $P_{Rotaxane}$ system show astonishing τ_h values of ≈1000 ms, which compares to electron lifetimes found in *n*-DSSC. This trend in τ_h is also reflected in the differences in PCEs, with the $P_{Rotaxane}$ 3-NDI-ring (25 mM) system showing an increased PCE compared to P1 p-DSSCs using 1 M I^-/I_3^- (0.07% vs 0.06%). Hence, despite the 40× lower concentration of 3-NDI-ring the current device has an increased performance compared to that based on the benchmark I^-/I_3^- electrolyte. The increased PCE for the $P_{rotaxane}$ 3- NDI-ring p-DSSC implies that recombination-dominating losses in P1-based *p*-DSSC are addressable by invoking a supramolecular electronic approach. The results of the increased performance of $P_{Rotaxane}$-based *p*-DSSC are consistent with the fs-TA results that suggest that an additional 3-NDI-ring in the electrolyte possibly acts as an electron acceptor. Although the difference in time constants relative to the system in electrolytes without an additional 3-NDI-ring is small, the effects can be significant. Beneficial effects possibly arise from the 3-NDI-ring in the electrolyte promoting hole injection by $P_{Rotaxane}^*$ into the NiO or accepting an electron from $P_{Rotaxane}^{\bullet-}$. In all cases, the implementation of dye-mediator interactions leads to extended hole lifetimes.

2.6. Inhibiting Recombination

To demonstrate that we inhibited the recombination, we are determining the theoretical maximum current that we can expect in our device (J_{lim}) based on the redox mediator of choice and its concentration. From the concentration and diffusion coefficient of the redox mediator, we can determine the mass transfer. The J_{lim} is independent of the dye system and is solely dictated by the properties of the electrolyte, (thus J_{lim} is not photocurrent, just current). The calculated J_{lim} is compared with the photocurrents at short circuit that we observe (J_{SC}) in our supramolecular dye-system (3-NDI-ring/3-NDI-ring$^{\bullet-}$) and traditional iodide-systems (I^-/I_3^-). (see Section S3.10, Supporting Information) based on the I^-/I_3^- and the 3-NDI-ring electrolyte.

By approximation, the solar cells based on the 3-NDI-ring electrolyte (12.5:12.5 mM, 3-NDI-ring/3-NDI-ring$^{\bullet-}$) have maximum photocurrent densities of $J_{lim(3\text{-}NDI\text{-}ring)} = 0.6$ mA cm^{-2} while that of the I^-/I_3^- cells are around $J_{lim(I3\text{-})} = 95$ mA cm^{-2}.[65] This means that under these conditions the *p*-DSSCs employing the 3-NDI-ring reach as much as 60–70% of the theoretical current for the devices based on $P_{Stopper}$ and $P_{Rotaxane}$ respectively, while for cells based on the I^-/I_3^- (0.9:0.1 M) this is only 1.6%. The fact that the obtained photocurrents approach the limited current, implies that recombination has been suppressed to a minimum and the system based on supramolecular interactions is mostly limited by slow diffusion of the large macrocyclic mediator. This improvement in maximum photocurrent densities is not just an improvement as a result of surface shielding by using a bigger electrolyte as P1 combined with 3-NDI-ring approaches 20% of the theoretically achievable current. Despite $P_{Rotaxane}$ dye loading being 50% less than that of P1, the rotaxane system manages improvements in approaching the J_{lim}. Both the measured τ_h and the calculated maximum photocurrent demonstrate that recombination is suppressed to a minimum, implying that the system is mostly limited by low solubility and slow diffusion of the large macrocyclic mediator.

3. Conclusion

In conclusion, we report a nanoengineered dye-regeneration system $P_{Rotaxane}$, where a macrocyclic electron acceptor is permanently bound via rotaxane formation in close proximity to the dye. Femtosecond transient absorption spectroscopy revealed ultrafast (211 ± 7 fs and 2.92 ± 0.05 ps) charge transfer from the $P_{Rotaxane}$ dye to the permanently bound mediator (3-NDI-ring). Utilization of rotaxane topologies leads to *p*-DSSCs with unprecedented hole lifetimes, suppressing charge recombination to a large extent, and providing photocurrents up to 70% of the

theoretical maximum. We are currently pursuing the integration of this strategy with broader absorbing, high-efficiency dyes, which should lead to a new generation of supramolecular *p–n* junctions that engender charge rectification in photovoltaics.

Supporting Information

Supporting Information is available from the Wiley Online Library or from the author.

Acknowledgements

The authors would like to thank Marie Brands for her assistance with the TA measurements and Prof. Elizabeth von Hauff for her advice on the EIS measurements. This study was supported by the Holland Research School for Molecular Sciences (HRSMC) and the University of Amsterdam. A part of this study was supported by Merck GmbH and the Dutch National Science Foundation (NWO) for funding The TA data was supported by the Advanced Research Center for Chemical Building Blocks, ARC CBBC, which is co-founded and co-financed by the Netherlands Organization for Scientific Research (NWO) and the Netherlands Ministry of Economic Affairs and Climate Policy.

Conflict of Interest

The authors declare no conflict of interest.

Data Availability Statement

The data that support the findings of this study are available from the corresponding author upon reasonable request.

Keywords

femtosecond transient absorption, interfacial photoelectrochemistry, *p*-type dye-sensitized solar cell, rotaxanes, supramolecular electronics

Received: December 4, 2023
Published online:

[1] H. H. Mcgarraugh, W. Liu, B. P. Matthews, B. D. Smith, *Eur. J. Org. Chem.* **2019**, *2019*, 3489.
[2] T. H. Ngo, J. Labuta, G. N. Lim, W. A. Webre, F. D'souza, P. A. Karr, J. E. M. Lewis, J. P. Hill, K. Ariga, S. M. Goldup, *Chem. Sci.* **2017**, *8*, 6679.
[3] E. Arunkumar, N. Fu, B. D. Smith, *Chemistry* **2006**, *12*, 4684.
[4] Y. Goto, T. Hisatomi, Q. Wang, T. Higashi, K. Ishikiriyama, T. Maeda, Y. Sakata, S. Okunaka, H. Tokudome, M. Katayama, S. Akiyama, H. Nishiyama, Y. Inoue, T. Takewaki, T. Setoyama, T. Minegishi, T. Takata, T. Yamada, K. Domen, *Joule* **2018**, *2*, 509.
[5] H. Li, A. C. Fahrenbach, A. Coskun, Z. Zhu, G. Barin, Y.-L. Zhao, Y. Y. Botros, J.-P. Sauvage, J. F. Stoddart, *Angew. Chem., Int. Ed.* **2011**, *50*, 6782.
[6] C. W. Fuller, P. S. Padayatti, H. Abderrahim, L. Adamiak, N. Alagar, N. Ananthapadmanabhan, J. Baek, S. Chinni, C. Choi, K. J. Delaney, R. Dubielzig, J. Frkanec, C. Garcia, C. Gardner, D. Gebhardt, T. Geiser, Z. Gutierrez, D. A. Hall, A. P. Hodges, G. Hou, S. Jain, T. Jones, R. Lobaton, Z. Majzik, A. Marte, P. Mohan, P. Mola, P. Mudondo, et al., *Proc. Natl. Acad. Sci. USA* **2022**, *119*, 2112812119.
[7] V. K. Sangwan, R. P. Ortiz, J. M. P. Alaboson, J. D. Emery, M. J. Bedzyk, L. J. Lauhon, T. J. Marks, M. C. Hersam, *ACS Nano* **2012**, *6*, 7480.
[8] C. Zheng, Y. Liao, S.-T. Han, Y. Zhou, *Adv. Electron. Mater.* **2020**, *6*, 2000641.
[9] L. Wang, L. Wang, L. Zhang, D. Xiang, in *Molecular-Scale Electronics: Current Status and Perspectives* (Ed: X. Guo), Springer, Cham, Switzerland **2019**, pp. 45–86.
[10] K. Wang, E. Meyhofer, P. Reddy, *Adv. Funct. Mater.* **2020**, *30*, 1904534.
[11] D. Xiang, X. Wang, C. Jia, T. Lee, X. Guo, *Chem. Rev.* **2016**, *116*, 4318.
[12] S. V. Aradhya, L. Venkataraman, *Nat. Nanotechnol.* **2013**, *8*, 399.
[13] N. Xin, J. Guan, C. Zhou, X. Chen, C. Gu, Y. Li, M. A. Ratner, A. Nitzan, J. F. Stoddart, X. Guo, *Nat. Rev. Phys.* **2019**, *1*, 211.
[14] Y. Liu, X. Qiu, S. Soni, R. C. Chiechi, *Chem. Phys. Rev.* **2021**, *2*, 021303.
[15] H. Chen, J. Fraser Stoddart, *Nat. Rev. Mater.* **2021**, *6*, 804.
[16] D. C. Milan, M. Krempe, A. K. Ismael, L. D. Movsisyan, M. Franz, I. Grace, R. J. Brooke, W. Schwarzacher, S. J. Higgins, H. L. Anderson, C. J. Lambert, R. R. Tykwinski, R. J. Nichols, *Nanoscale* **2017**, *9*, 355.
[17] P. Lussis, T. Svaldo-Lanero, A. Bertocco, C.-A. Fustin, D. A. Leigh, A.-S. Duwez, *Nat. Nanotechnol.* **2011**, *6*, 553.
[18] H. Wen, W. Li, J. Chen, G. He, L. Li, M. A. Olson, A. C.-H. Sue, J. F. Stoddart, X. Guo, *Sci. Adv.* **2016**, *2*, 1601113.
[19] Y. Luo, C. P. Collier, J. O. Jeppesen, K. A. Nielsen, E. Deionno, G. Ho, J. Perkins, H.-R. Tseng, T. Yamamoto, J. F. Stoddart, J. R. Heath, *ChemPhysChem* **2002**, *3*, 519.
[20] J.-H. Tang, Y. Li, Q. Wu, Z. Wang, S. Hou, K. Tang, Y. Sun, H. Wang, H. Wang, C. Lu, X. Wang, X. Li, D. Wang, J. Yao, C. J. Lambert, N. Tao, Y.-W. Zhong, P. J. Stang, *Nat. Commun.* **2019**, *10*, 4599.
[21] C. Zhou, X. Li, Z. Gong, C. Jia, Y. Lin, C. Gu, G. He, Y. Zhong, J. Yang, X. Guo, *Nat. Commun.* **2018**, *9*, 807.
[22] Y. Han, C. Nickle, Z. Zhang, H. P. A. G. Astier, T. J. Duffin, D. Qi, Z. Wang, E. Del Barco, D. Thompson, C. A. Nijhuis, *Nat. Mater.* **2020**, *19*, 843.
[23] B. H. Farnum, K.-R. Wee, T. J. Meyer, *Nat. Chem.* **2016**, *8*, 845.
[24] H. Tian, J. Oscarsson, E. Gabrielsson, S. K. Eriksson, R. Lindblad, B. Xu, Y. Hao, G. Boschloo, E. M. J. Johansson, J. M. Gardner, A. Hagfeldt, H. Rensmo, L. Sun, *Sci. Rep.* **2014**, *4*, 4282.
[25] B. O'regan, M. Grätzel, *Nature* **1991**, *353*, 737.
[26] Y. Ren, D. Zhang, J. Suo, Y. Cao, F. T. Eickemeyer, N. Vlachopoulos, S. M. Zakeeruddin, A. Hagfeldt, M. Grätzel, *Nature* **2023**, *613*, 60.
[27] E. Benazzi, J. Mallows, G. H. Summers, F. A. Black, E. A. Gibson, *J. Mater. Chem. C* **2019**, *7*, 10409.
[28] I. R. Perera, T. Daeneke, S. Makuta, Z. Yu, Y. Tachibana, A. Mishra, P. Bäuerle, C. A. Ohlin, U. Bach, L. Spiccia, *Angew. Chem., Int. Ed.* **2015**, *54*, 3758.
[29] T. Daeneke, Z. Yu, G. P. Lee, D. Fu, N. W. Duffy, S. Makuta, Y. Tachibana, L. Spiccia, A. Mishra, P. Bäuerle, U. Bach, *Adv. Energy Mater.* **2015**, *5*, 1401387.
[30] C. J. Wood, G. H. Summers, E. A. Gibson, *Chem. Commun.* **2015**, *51*, 3915.
[31] J. J. Leung, J. Warnan, D. H. Nam, J. Z. Zhang, J. Willkomm, E. Reisner, *Chem. Sci.* **2017**, *8*, 5172.
[32] T. E. Rosser, M. A. Gross, Y.-H. Lai, E. Reisner, *Chem. Sci.* **2016**, *7*, 4024.
[33] F. Li, K. Fan, B. Xu, E. Gabrielsson, Q. Daniel, L. Li, L. Sun, *J. Am. Chem. Soc.* **2015**, *137*, 9153.
[34] J. He, H. Lindström, A. Hagfeldt, S.-E. Lindquist, *J. Phys. Chem. B* **1999**, *103*, 8940.
[35] L. D'Amario, L. J. Antila, B. Pettersson Rimgard, G. Boschloo, L. Hammarström, *J. Phys. Chem. Lett.* **2015**, *6*, 779.
[36] S. Mori, S. Fukuda, S. Sumikura, Y. Takeda, Y. Tamaki, E. Suzuki, T. Abe, *J. Phys. Chem. C* **2008**, *112*, 16134.
[37] S. Nakade, Y. Saito, W. Kubo, T. Kitamura, Y. Wada, S. Yanagida, *J. Phys. Chem. B* **2003**, *107*, 8607.
[38] F. Odobel, Y. Pellegrin, E. A. Gibson, A. Hagfeldt, A. L. Smeigh, L. Hammarström, *Coord. Chem. Rev.* **2012**, *256*, 2414.

[39] A. Morandeira, G. Boschloo, A. Hagfeldt, L. Hammarström, *J. Phys. Chem. B* **2005**, *109*, 19403.
[40] A. Nattestad, M. Ferguson, R. Kerr, Y.-B. Cheng, U. Bach, *Nanotechnology* **2008**, *19*, 295304.
[41] F. G. L. Parlane, C. Mustoe, C. W. Kellett, S. J. Simon, W. B. Swords, G. J. Meyer, P. Kennepohl, C. P. Berlinguette, *Nat. Commun.* **2017**, *8*, 1761.
[42] S. J. C. Simon, F. G. L. Parlane, W. B. Swords, C. W. Kellett, C. Du, B. Lam, R. K. Dean, K. Hu, G. J. Meyer, C. P. Berlinguette, *J. Am. Chem. Soc.* **2016**, *138*, 10406.
[43] F. A. Black, C. A. Clark, G. H. Summers, I. P. Clark, M. Towrie, T. Penfold, M. W. George, E. A. Gibson, *Phys. Chem. Chem. Phys.* **2017**, *19*, 7877.
[44] Y. Uemura, T. N. Murakami, N. Koumura, *J. Phys. Chem. C* **2014**, *118*, 16749.
[45] W. B. Swords, S. J. C. Simon, F. G. L. Parlane, R. K. Dean, C. W. Kellett, K. Hu, G. J. Meyer, C. P. Berlinguette, *Angew. Chem., Int. Ed.* **2016**, *55*, 5956.
[46] T. Bouwens, S. Mathew, J. N. H. Reek, *Faraday Discuss.* **2019**, *215*, 393.
[47] T. Bouwens, T. M. A. Bakker, K. Zhu, J. Hasenack, M. Dieperink, A. M. Brouwer, A. Huijser, S. Mathew, J. N. H. Reek, *Nat. Chem.* **2023**, *15*, 213.
[48] V. V. Pavlishchuk, A. W. Addison, *Inorg. Chim. Acta* **2000**, *298*, 97.
[49] N. G. Connelly, W. E. Geiger, *Chem. Rev.* **1996**, *96*, 877.
[50] P. Thordarson, *Chem. Soc. Rev.* **2011**, *40*, 1305.
[51] P. Qin, J. Wiberg, E. A. Gibson, M. Linder, L. Li, T. Brinck, A. Hagfeldt, B. Albinsson, L. Sun, *J. Phys. Chem. C* **2010**, *114*, 4738.
[52] K. Zhu, S. K. Frehan, A. M. Jaros, D. B. O'neill, J. P. Korterik, K. Wenderich, G. Mul, A. Huijser, *J. Phys. Chem. C* **2021**, *125*, 16049.
[53] K. Zhu, S. K. Frehan, G. Mul, A. Huijser, *J. Am. Chem. Soc.* **2022**, *144*, 11010.
[54] Q. Pan, L. Freitag, T. Kowacs, J. C. Falgenhauer, J. P. Korterik, D. Schlettwein, W. R. Browne, M. T. Pryce, S. Rau, L. González, J. G. Vos, A. Huijser, *Chem. Commun.* **2016**, *52*, 9371.
[55] A. Trabolsi, N. Khashab, A. C. Fahrenbach, D. C. Friedman, M. T. Colvin, K. K. Cotí, D. Benítez, E. Tkatchouk, J.-C. Olsen, M. E. Belowich, R. Carmielli, H. A. Khatib, W. A. Goddard, M. R. Wasielewski, J. F. Stoddart, *Nat. Chem.* **2010**, *2*, 42.
[56] K. Saito, A. W. Rutherford, H. Ishikita, *Proc. Natl. Acad. Sci. USA* **2013**, *110*, 954.
[57] C. J. Wood, G. H. Summers, C. A. Clark, N. Kaeffer, M. Braeutigam, L. R. Carbone, L. D'amario, K. Fan, Y. Farré, S. Narbey, F. Oswald, L. A. Stevens, C. D. J. Parmenter, M. W. Fay, A. La Torre, C. E. Snape, B. Dietzek, D. Dini, L. Hammarström, Y. Pellegrin, F. Odobel, L. Sun, V. Artero, E. A. Gibson, *Phys. Chem. Chem. Phys.* **2016**, *18*, 10727.
[58] L. D'amario, J. Föhlinger, G. Boschloo, L. Hammarström, *Chem. Sci.* **2018**, *9*, 223.
[59] H. Tian, Z. Yu, A. Hagfeldt, L. Kloo, L. Sun, *J. Am. Chem. Soc.* **2011**, *133*, 9413.
[60] A. Yella, S. Mathew, S. Aghazada, P. Comte, M. Grätzel, M. K. Nazeeruddin, *J. Mater. Chem. C* **2017**, *5*, 2833.
[61] J. J. Nelson, T. J. Amick, C. M. Elliott, *J. Phys. Chem. C* **2008**, *112*, 18255.
[62] F. Fabregat-Santiago, G. Garcia-Belmonte, I. Mora-Seró, J. Bisquert, *Phys. Chem. Chem. Phys.* **2011**, *13*, 9083.
[63] Z. Huang, G. Natu, Z. Ji, P. Hasin, Y. Wu, *J. Phys. Chem. C* **2011**, *115*, 25109.
[64] R. D. Shannon, *Acta Crystallogr. A* **1976**, *32*, 751.
[65] J. Halme, P. Vahermaa, K. Miettunen, P. Lund, *Adv. Mater.* **2010**, *22*, E210.

